Examination of C12A7 electride work function and surface composition by means of XPS, UPS and thermionic emission measurements

Antonio Gurciullo, Vasiliki Papaefthimiou, Paul Lascombes, Stéphane Mazouffre, Fabian Plaza, Angel Post

▶ **To cite this version:**

Antonio Gurciullo, Vasiliki Papaefthimiou, Paul Lascombes, Stéphane Mazouffre, Fabian Plaza, et al.. Examination of C12A7 electride work function and surface composition by means of XPS, UPS and thermionic emission measurements. 37th International Electric Propulsion Conference, Jun 2022, Cambridge, United States. hal-03797369

HAL Id: hal-03797369
https://hal.science/hal-03797369

Submitted on 4 Oct 2022

HAL is a multi-disciplinary open access archive for the deposit and dissemination of scientific research documents, whether they are published or not. The documents may come from teaching and research institutions in France or abroad, or from public or private research centers.

L'archive ouverte pluridisciplinaire **HAL**, est destinée au dépôt et à la diffusion de documents scientifiques de niveau recherche, publiés ou non, émanant des établissements d'enseignement et de recherche français ou étrangers, des laboratoires publics ou privés.

Examination of C12A7 electride work function and surface composition by means of XPS, UPS and thermionic emission measurements

IEPC-2022- 104

Presented at the 37th International Electric Propulsion Conference
Massachusetts Institute of Technology, Cambridge, MA USA
June 19-23, 2022

Antonio Gurciullo[1]
Exotrail, Massy, 91300, France

Vasiliki Papaefthimiou[2]
ICPEES, Université de Strasbourg, Schiltigheim, 67087, France

Paul Lascombes[3]
Exotrail, Massy, 91300, France

Stéphane Mazouffre[4]
ICARE, CNRS, Orléans, 45071, France

Fabian Plaza[5] and Angel Post[6]
Advanced Thermal Devices, Madrid, 28925, Spain

The work functions of LaB_6 and C12A7:e- samples have been estimated by thermionic emission measurements and compared with ultraviolet photoelectron spectroscopy (UPS) data. In addition to this, the surface composition of the samples is characterized by X-ray photoelectron spectroscopy (XPS). Consistent work function values of 3.2-3.3 eV have been measured for clean LaB_6 samples. A wider range of values has been measured with the C12A7:e- sample, where a work function of 2.4-2.8 eV and 3.2 eV is estimated when using a setup for thermion emission and UPS, respectively.

I. Nomenclature

A_0 = Richardson-Dushman constant, $120\,\frac{A}{cm^2K}$
C = Constant
e = Elementary charge, $1.6 \cdot 10^{-19}\mathrm{C}$
J = Current density
k_B = Boltzmann constant, $\approx 1.38 \cdot 10^{-23}\mathrm{m^2kg\,s^{-2}K^{-1}}$
T = Sample temperature

[1] VP Propulsion, Propulsion, antonio.gurciullo@exotrail.com
[2] Project Engineer, papaefthymio@unistra.fr
[3] Chief Scientist, paul.lascombes@exotrail.com
[4] Directeur de Recherche, ICARE, CNRS, stephane.mazouffre@cnrs-orleans.fr.
[5] General Manager, jfplaza@atdevices.com.
[6] Space and Defense Director, apost@atdevices.com

Copyright © 2022 by Exotrail. Published by the Electric Rocket Propulsion Society with permission.

UPS = Ultraviolet photoelectron spectroscopy
XPS = X-ray photoelectron spectroscopy
WF = Work function

β Constant of the temperature-dependent work function
ϕ Temperature-dependent work function
ϕ_{eff} Effective work function
ϕ_0 Work function

II. Introduction

Conventional cathodes for electric propulsion applications take advantage of thermionic materials such as lanthanum hexaboride (LaB6) and tungsten impregnated barium oxide (BaO). At the same time, the stringent demand of reduced cathode operating temperature, higher efficiency and higher robustness to impurities and reactive propellants encouraged research toward novel methods and thermionic materials [1]. Research efforts have focused on the electride of 12 CaO·7 Al2O3 (C12A7) for thermionic material application.

The compound C12A7 is member of the calcium aluminate mixed-compound systems and its unit cell is [Ca24Al28O64]4+(O2-)2 [2]. It has a peculiar crystal structure in which extra-framework oxygen ions (O2-) are loosely bond to the calcium atoms of the framework. These extra-framework ions are substituted by electrons through reduction methods and the unit cell takes the form [Ca24Al28O64]4+(e-)4, commonly known as C12A7:e- or C12A7 electride.

This electride is stable at ambient atmosphere and temperature thanks to the framework structure that protects the extra-framework electrons from reacting with oxygen and water vapour. In the electric propulsion community, interest on C12A7:e- has recently raised due to the reported low work function, chemical stability and potential compatibility with iodine [3].

However, literature offers contradictory findings about the C12A7:e- work function. Field emission tests at room temperature have shown a work function of 0.6 eV [4], in high temperature thermal field emission measurement the work function appeared to be 2.1 eV [5], ultraviolet photoemission spectroscopy (UPS) and photoelectron yield spectroscopy (PYS) agreed on a work function of 2.4 eV [6]. Another attempt made by UPS showed a value of 3.7eV [4]. Within the electric propulsion community, the C12A7:e- work function has been measured by thermionic diode setups, which have supposedly shown a value as low as 0.52eV [7], or emission current densities higher than those of LaB6 given a fixed emitter temperature [8].

The fabrication method, complicating surface layer effects [9], possible surface contamination during manipulation and test setup are the main factors influencing the results of the measured work function. In this paper, the work function of a C12A7:e- sample is measured with and compared among two different methods, namely UPS and thermionic diode emission. Prior to these tests, the surface chemical composition of the samples is investigated by X-ray photoemission spectroscopy (XPS). In parallel, LaB_6 samples are also tested and their emission properties are compared with those of the C12A7:e- sample using identical measurement setup, instruments and methodology.

III. Experimental setup

A. Samples description

A total of four samples are tested, two LaB_6 discs (here named LaB6-sample1 and LaB6-sample2) and two C12A7:e- discs (here named C12A7-sample1 and C12A7-sample2). Samples "1" of each thermionic material are dedicate to XPS and UPS measurements, while samples "2" are tested in the thermionic emission setup. Lanthanum hexaboride samples are discs of 8 mm in diameter and 2 mm of thickness produced by Sindlhauser Material GmbH. The C12A7:e- samples are manufactured by ATD in discs of 8 mm of diameter and 1 mm of thickness.

B. UPS/XPS setup

The UPS/XPS measurements were carried out in the ultrahigh vacuum (UHV) setup shown in Fig. 1 (base pressure $5x10^{-9}$ mbar) composed of several interconnected chambers. The analysis chamber is equipped with a VSW Class WA hemispherical electron analyzer (150 mm radius) with a multi-channeltron detector, two X-ray sources (dual and

monochromatic) and a differentially pumped UV photon source operating with He as discharge gas (He I, 21.21 eV, ca. 2 mm circular entrance slit).

The samples were firstly measured as received, using XPS and UPS. For this series of experiments, the samples were attached to the spectrometer holder using a conductive double-sided carbon adhesive tape. In order to understand the effect of various ex-situ (chemical cleaning) and in situ (annealing, Ar^+ sputtering) treatments on the surface composition and work function of LaB_6, a second series of experiments was performed, were this sample was subjected to the different treatments and the differences in its surface composition and work function were measured by means of XPS and UPS. The sample was placed using clips on a sample holder that could be heated. LaB_6 was first cleaned ex-situ, using 3 parts (15mL) of Hydrochloric acid (37% ACS reagent Grade) and 1 part (5 mL) of Nitric acid (70% ACS reagent grade). Then it was thoroughly rinsed with pure water and it was immediately attached to the spectrometer holder using clips and brought in UHV. The sample was annealed overnight at 300°C, to remove remaining H_2O. XPS was used to examine the surface state after this procedure. The sample was then cleaned by Ar+ sputtering (in the raster mode, I_{sample}=10 μA, E_{ions}=5 KeV, t_{total}= 3.5 h) to remove the remaining C/O from the surface. Small amounts of O and C persisted on the surface despite the cleaning procedure, because much higher annealing temperature (1600 K) and Ar^+ sputtering cleaning cycles are required to totally clean the LaB_6 surface [10].

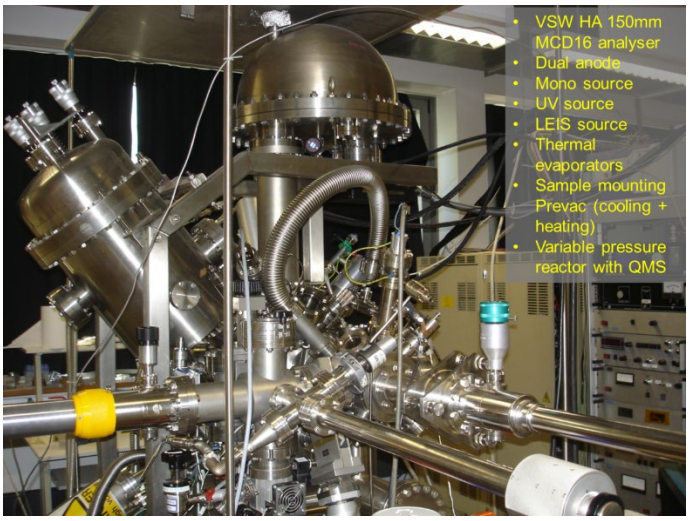

Fig. 1 Picture of the ultrahigh vacuum setup used for the XPS and UPS measurements.

C. Thermionic diode emission setup

The experimental setup includes the use of a vacuum chamber, a test hardware in which a sample is placed, a power supply and sourcemeter for voltage and current control, thermocouples and a LabVIEW software for data acquisition.

The vacuum chamber, named Astreos, is equipped with a temperature control unit (Lauda model Integral XT 280 W) for thermal-vacuum operation. The thermal system is used to maintain the chamber walls at a fixed temperature of 35°C during the tests. The vacuum chamber is equipped with a rough pump and a turbopump (Pfeiffer Vacuum model ATH 2300M) with pumping speed of 2150 l/s for N_2. The typical pressure during tests is in the range of $1 \cdot 10^{-6}$ to $8 \cdot 10^{-6}$ mbar, depending on the sample temperature.

The core of test hardware includes a pyrolytic boron nitride (PBN) heater from Neyco (model PCPBNR10), a boron nitride (BN) insulator, a tantalum (Ta) foil as cathode terminal, a soft graphite spacer and a tantalum disc as anode terminal. A structure made by steatite shoulder washers, stainless steel screws and molybdenum foils ensures mechanical clamp. A set of graphite plates optically shields the hottest part of the setup from the external environment.

A schematic of the core test hardware is depicted in Fig. 2. The sample (depicted in violet) is mechanically compressed by the BN (in white) on the 1 mm graphite spacer (in black) and Ta foil (in grey). The electrical contact between the sample and the cathode terminal (Ta foil) is ensured by this mechanical compression. A fixed compression force is assured by bolts screwed with known torque. Due to thermal dilatation, this compression force may change during the test. The top flat surface of the sample exposed to the anode is about 0.2827 cm^2 (6 mm in diameter) and it is distant 4.1 ± 0.1 mm from the anode disc.

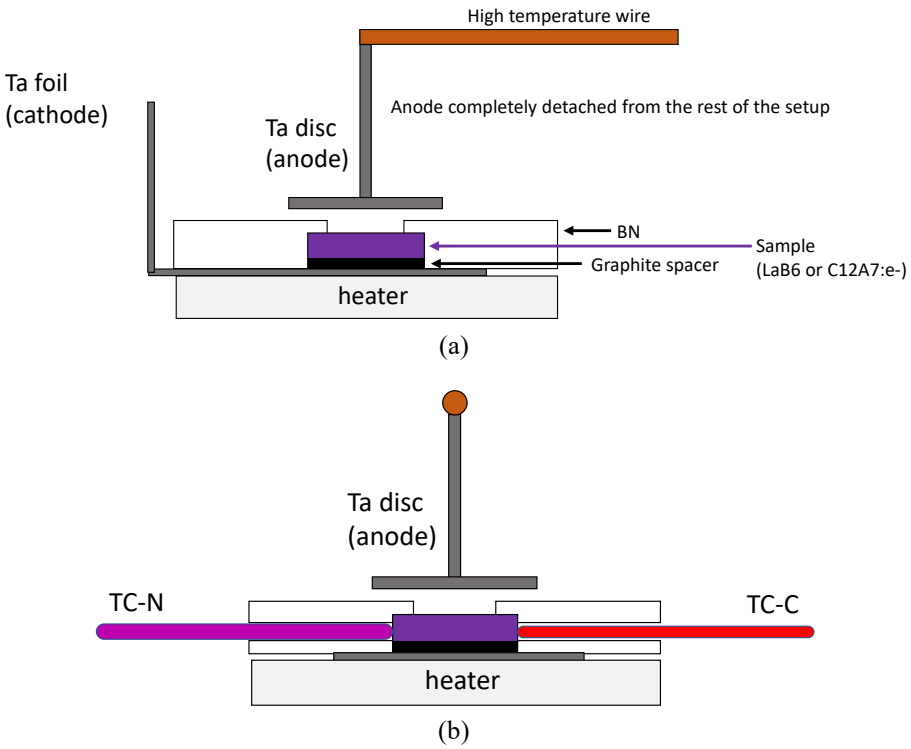

Fig. 2 Schematic of the core setup hardware. Figures (a) and (b) show two different sides.

The temperature of the sample is monitored by two thermocouples, which pass through two side holes (diameter of 1 mm) of the BN insulator. Both thermocouples are shielded and ungrounded. A thermocouple type N (TC-N), whose outer diameter is 1.1 mm, is used to control the heater power through a PID controller by a LabVIEW software. A thermocouple type C (TC-C) has an outer diameter of 0.9 mm. Due to the tight fit between the TC-N and the BN insulator, its measured temperature is equal or lower than that measured by the TC-C, which is in a loose contact with the BN insulator while ensuring a good mechanical contact with the sample. The here reported sample temperature is that measured by TC-C. Pictures of the setup are shown in Fig. 3.

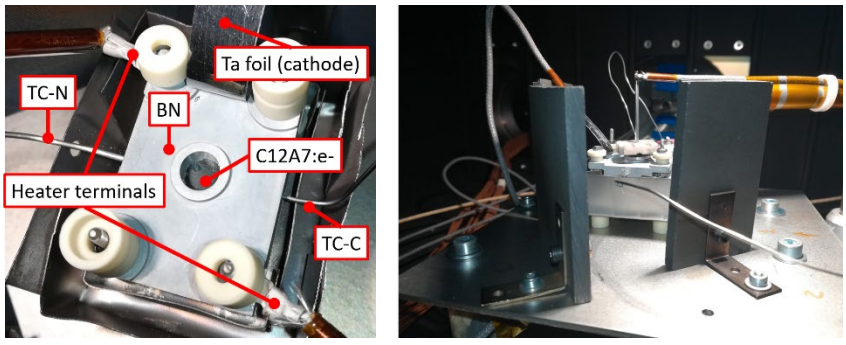

Fig. 3 Pictures of the thermionic emission setup.

The list of laboratory equipment and software employed in the tests is shown in Table 1.

Table 1 List of equipment.

Equipment name	Model	Specifications
Sourcemeter	Keithley 2410	0-1000 V (programming resolution of 50mV) 20 mA maximum current (measurement resolution of 100 nA)
Heater power supply	Keithley 2260B-80-27	80V, 27A, 720W
TC-N reader	Omega TC-08	-
TC-C reader	ECO-24 PMA	-
PID software	LabVIEW code	Custom software made by Exotrail

Schematics of the electrical and measurement acquisition setup are depicted in Fig. 4. The cathode electrode (C) and the low voltage branch of the heater (H-) are grounded to the facility. The anode electrode (A) and the cathode electrode – electrically in contact with the sample – are connected to the sourcemeter, which is controlled as a voltage source by the LabVIEW software. The heater is connected to a high-current power supply and controlled in current limited mode. The heater current is established by a PID controller included into the custom LabVIEW software, which monitors the sample temperature read by the TC-N reader (Omega TC-08). A second thermocouple reader (ECO-24 PMA) displays the sample temperature measured by the TC-C.

.

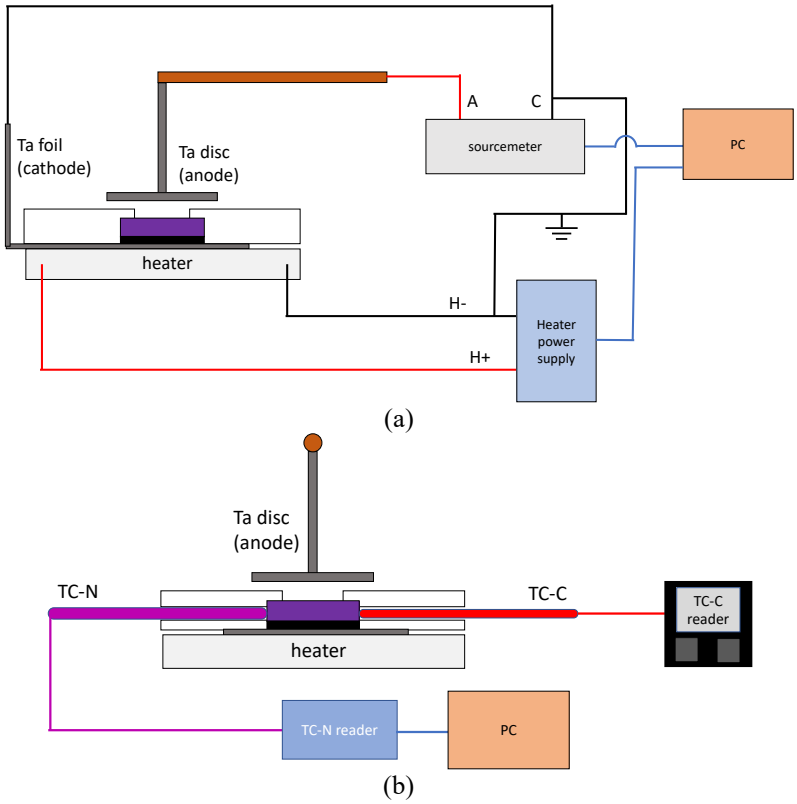

Fig. 4 Schematic of the electrical and measurement acquisition setup.

IV. Test methodology and data analysis

A. UPS

For the UPS measurements, the He I excitation energy ($h\nu$=21.2 eV) and a Constant Retarding Ratio (CRR=10) analyzer operation mode were used. The measurements were performed by applying four different external negative bias voltages of -10, -15, -20 and -28V to the samples, in order to separate sample and analyzer spectral cutoffs, and to increase the secondary electron yield. The electronic work function (WF) is calculated by measuring the difference between the high binding energy threshold of the UPS spectrum and the excitation energy (i.e. 21.2 eV), assuming that the Fermi Levels (E_F) of the spectrometer and the samples are aligned.

B. XPS

For the XPS measurements, the monochromatic Al Kα line at 1486.6 eV was used (anode operating at 240 W). The spectrometer was calibrated to yield the standard Cu $2p_{3/2}$ line at 932.70 eV and the Au $4f_{7/2}$ line at 84.00 eV. The X-ray incident angle is 45 degrees with respect to the sample and the collecting angle of the analyzer was 0 degrees to the surface normal. A survey scan was initially acquired to determine the elements present. This was followed by high resolution scans of the major elements. The constant pass energy mode was used to record both survey and high resolution spectra (90 and 44 eV respectively). The Casa XPS software was used for the analysis of the data in all cases. The error in the measured / calculated binding energy values is estimated ±0.05 eV. It is noteworthy to mention that the probing depth (sometimes also called as information or sampling depth) is estimated ca. 0.3 and 5-10 nm for UPS and XPS respectively, based on the photoelectron kinetic energy values [11].

C. Thermionic emission

The sample, encased within the thermionic emission setup, is placed within the Astreos vacuum chamber, which is pumped with a turbopump overnight to allow proper outgassing. The typical pressure is in the range of 10^{-6} to $8 \cdot 10^{-6}$ mbar, depending on the sample temperature. After letting the setup outgassing overnight, the thermal case of the vacuum chamber is maintained at 35°C by the thermal management system. Further outgassing is performed for about 2h at sample temperature of about 500°C or above. Once the background pressure stabilises, the measurements are performed.

The sample being grounded to the facility, the anode is biased positively to collect the emitted electrons. The bias voltage sweeps from 8V to 1000V with a step of 8V. At each voltage step, the sourcemeter waits 5 s before recording the current. A total of two voltage sweeps are performed and the current values are averaged accordingly.

The current-voltage characteristic is recorded at various sample temperatures. To maintain the experimental conditions as congruent as possible between the various samples' tests, the heater power can deviate within 2 W at each sample temperature point. The first I-V measurement is performed at the highest temperature allowed by the sample or the heater setup, then the I-V characteristics are recorder for lower temperature with a temperature step of 25°C (TC-N). At each temperature step, the monitor system waits 180 seconds before starting the I-V characteristic acquisition. During this acquisition, the PID controller is disables to avoid the influence of a heater current change into the measurement.

Before the tests with the samples, the leak current of the system (without samples) is measured. This is subtracted from the I-V curves of the samples.

The heater power and the corresponding samples temperature are listed in Table 2.

Table 2 Heater power and sample temperature.

		TC-C, °C		
Heater power, W	**TC-N, °C**	**No sample**	**LaB_6**	**C12A7**
142	**785**	792	787	793
157	**810**	823	812	819
169	**835**	846	834	845
184	**860**	871	859	870
201	**885**	898	889	900
216	**910**	933	916	-
234	**935**	956	948	-

An example of raw I-V characteristics of the C12A7:e- sample (ATD, C12A7_2) is shown in Fig. 5.

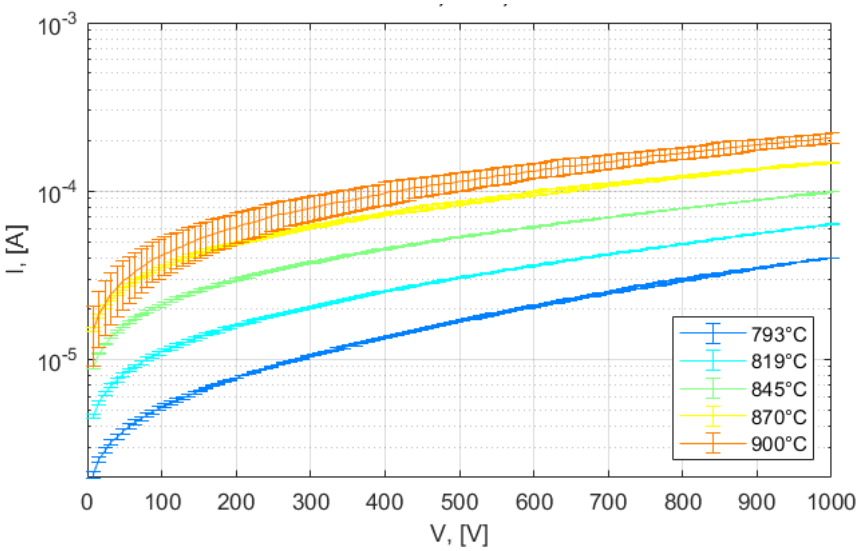

Fig. 5 Raw I-V characteristic of the C12A7:e- sample.

The data processing starts by subtracting the leak current contribution from the I-V characteristic of the sample. The obtained current is used for analysis. The leak current as a function of the bias voltage and heater power is shown in Fig. 6.

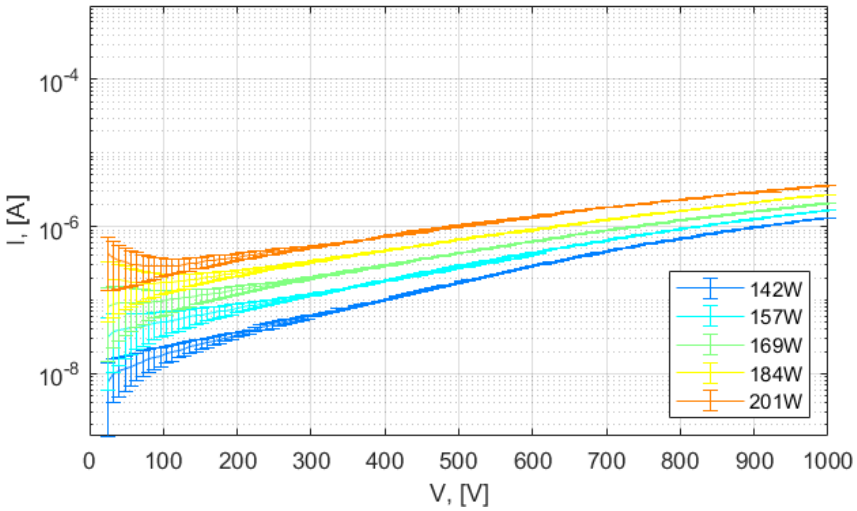

Fig. 6 Leak current as a function of the bias voltage and heater power.

The data processing is based on the interpretation of the Richardson-Dushman equation [12], where the thermionic current density J is a function of the effective work function ϕ_{eff} and the sample temperature T:

$$J = A_0 T^2 e^{-e\phi_{eff}/k_B T}, \tag{1}$$

where $A_0 = 120 \frac{A}{cm^2 K}$ is the Richardson-Dushman constant, e is the elementary charge and k_B is the Boltzmann constant. In the presence of a high electric field in the proximity of the thermionic surface, the effective work function is decreased. This phenomenon is called the Schottky effect [13], which is described by the following equation:

$$\phi_{eff} = \phi - \sqrt{\frac{eE_c}{4\pi\varepsilon_0}}, \tag{2}$$

where ϕ is the temperature-dependent work function, E_c is the electric field and ε_0 is the vacuum dielectric constant. Substituting equation (2) in equation (1), and considering that the electric field is a function of the electric potential, $E \approx V/d$, we derive the following relationship:

$$\begin{aligned} J &= A_0 T^2 \exp\left(-\frac{e\phi}{k_B T}\right) \exp\left(\frac{e}{k_B T}\sqrt{\frac{eE_c}{4\pi\varepsilon_0}}\right) \approx \\ &\approx A_0 T^2 \exp\left(-\frac{e\phi}{k_B T}\right) \exp\left(\frac{C\sqrt{V}}{T}\right), \end{aligned} \tag{3}$$

where C is a constant. The fist exponential term of equation (3), is the current density when $V = 0$ V:

$$J_0 = A_0 T^2 \exp\left(-\frac{e\phi}{k_B T}\right). \tag{4}$$

Thus, the logarithm of equation (3) is proportional to $\sqrt{V}$ as it follows:

$$\ln(J) \approx \ln(J_0) + \frac{C}{T}\sqrt{V}. \tag{5}$$

An example of the linear fit of equation (5) (dotted lines) is shown in Fig. 7, where the logarithm of the current density is a linear function of $\sqrt{V}$ above about 225 V (15 $\sqrt{\text{V}}$). The fitted curves, which are nonlinear as we are in the space charge limit regime (Child-Langmuir regime), allow the estimation of $\ln(J_0)$ and, thus, of J_0, which will be needed later.

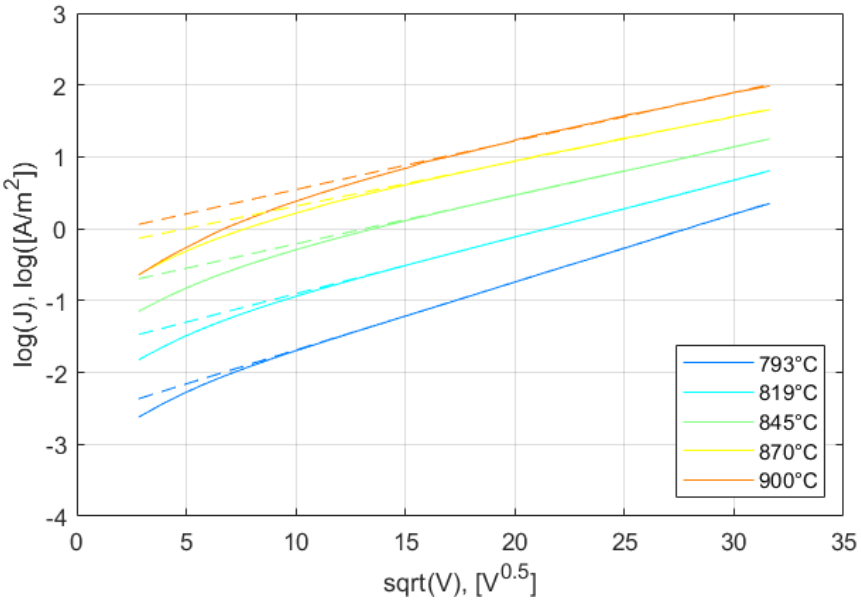

Fig. 7 . $ln(J)$ as a function of $\sqrt{V}$ of the C12A7:e- sample (C12A7-sample2), after the leak current has been subtracted. Above about 225 V (15 $\sqrt{V}$), the curve is a linear function of $\sqrt{V}$, and, as shown in equation (5), the dotted lines represent the fitted curves of these linear portions.

Note that the temperature-dependent work function can be expressed as a linear function of the sample temperature T [14]:

$$\phi = \phi_0 + \beta T, \tag{6}$$

where ϕ_0 is the work function and β is a constant. Substituting equation (6) in equation (4) we obtain

$$J_0 = A_0 \exp(-e\beta/k_B)\, T^2 \exp(-e\phi_0/k_B T), \tag{7}$$

where $D = A_0 \exp(-e\beta/k_B)$ is the temperature-modified Richardson constant. We can also write equation (7) as

$$\ln\left(\frac{J_0}{T^2}\right) - \ln(A_0) = -\frac{e\phi_0}{k_B T} - \frac{e\beta}{k_B}, \tag{8}$$

where J_0 is estimated by the fitting procedure shown in equation (5) and Fig. 7. Being the left-hand side of equation (8) known, a linear fitting of the right-hand side of the equation allows the calculation of the work function ϕ_0 and the coefficient β. An example of the linear fit, expressed as in equation (9) is shown in Fig. 8,

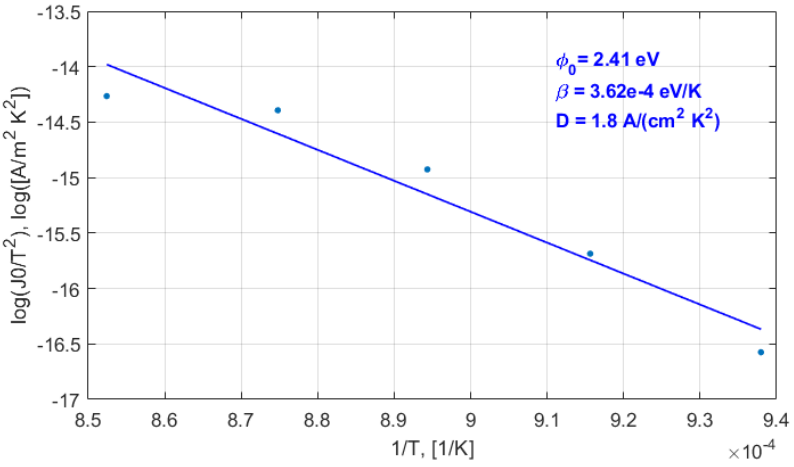

Fig. 8 Linear fit of equation (9) of the data of the C12A7:e- sample.

$$\ln\left(\frac{J_0}{T^2}\right) = \ln(A_0) - \frac{e\phi_0}{k_B T} - \frac{e\beta}{k_B}. \tag{9}$$

A similar post-processing method widely used in literature is that to assume that the effective work function is independent of the sample temperature, i.e. $\beta = 0$ eV/K in equation (9) before performing the linear fit. This approach forces the intercept of the vertical axis equal to $\ln(A_0)$, whatever the slope of the fitting curve (i.e. independently from ϕ_0). An example of comparison between the two fitting approaches is shown in Fig. 9, where the gap between the two work functions is 0.4 eV.

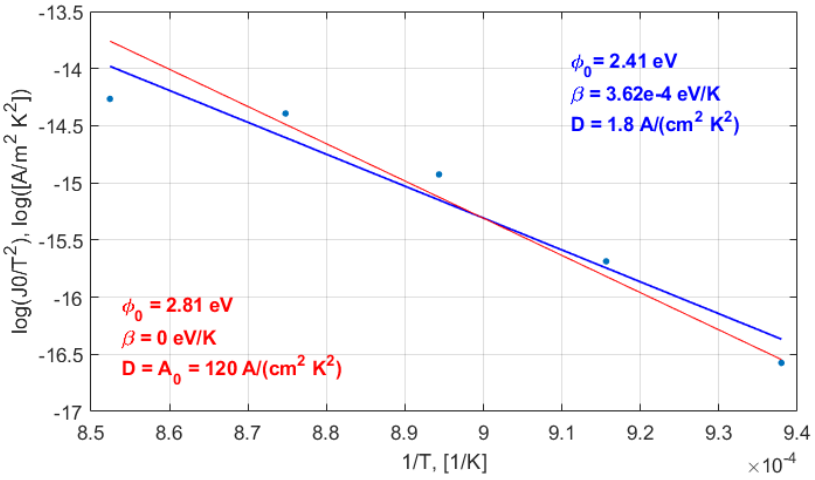

Fig. 9 Linear fit of equation (9) of the data of the C12A7:e- sample (C12A7-sample2) when $\beta = 0\ eV/K$ (red) and $\beta \neq 0\ eV/K$ (blue).

V. Results and discussion

A. UPS

The goal of this analysis was to establish the work function of the samples under different applied bias. The effect of various ex-situ (chemical cleaning) and in situ (annealing, Ar^+ sputtering) treatments on the work function of LaB_6 was also studied.

In the UPS spectra, the high binding energy cut-off (E_{vac}) was determined in all cases, as is depicted in the example of Fig. 10 for the electride. The E_{vac} values that were measured in this way, were plotted versus the applied voltage, and linear extrapolation to $E_{vac,0}$ was used for the determination of the surface Work Function (WF) of the electride [6], as is shown in Fig. 11. The WF of the non-treated LaB_6 was measured ca. 4.3 eV in all applied bias, a value that is well documented in the literature for oxygen exposed LaB_6 while after treatments the WF value was lower by 1.1 eV, in agreement with literature results [15].

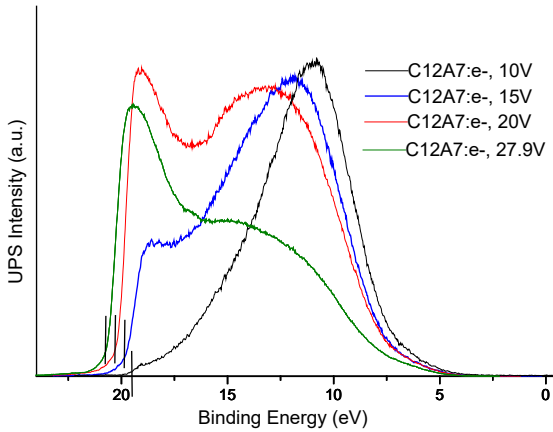

Fig. 10 UPS spectra of the C12A7:e- sample in different measuring bias. Determination of the high Binding Energy cut-off.

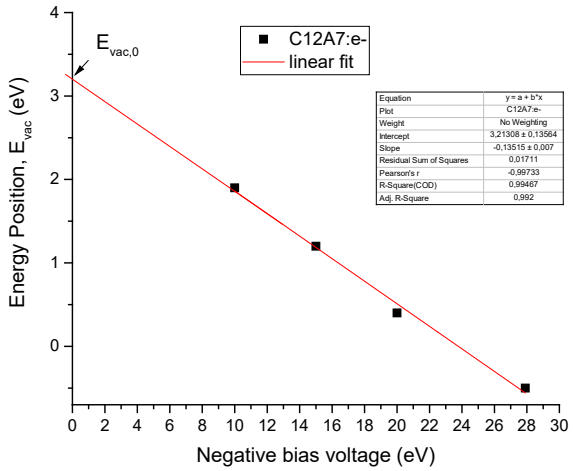

Fig. 11 Energy Position determined by UPS spectra versus bias for the electride sample. Determination of the surface Work Function (WF) by linear extrapolation to $E_{vac,0}$. The details of the linear fit are given in the inset of the graph.

B. XPS

XPS was employed to determine the oxidation/chemical state and composition of the elements in both samples and to understand the effect of various ex-situ (chemical cleaning) and in situ (annealing, Ar+ sputtering) treatments on the surface composition of LaB_6.

As marked in the survey scan spectra (Fig. 12), the following elements were detected on each sample surface: for LaB_6, there is oxygen, carbon, lanthanum and boron, while for C12A7:e- there is oxygen, carbon, calcium and aluminium. This result is an indirect confirmation of the samples purity, since it confirms that no unexpected/foreign species are present on the surface of the samples. The % surface ratio of all elements was calculated by using the area of the core level peaks recorded in the high-resolution scans, after normalization to the photoemission cross section and assuming a homogeneous distribution arrangement model. The obtained values are summarized in Table 3. From this table and the corresponding survey scan spectra it is evident that the surface carbon from contamination was drastically reduced after chemical cleaning and in-situ Ar^+ sputtering and annealing treatments of LaB_6 and that its surface was also enriched in B.

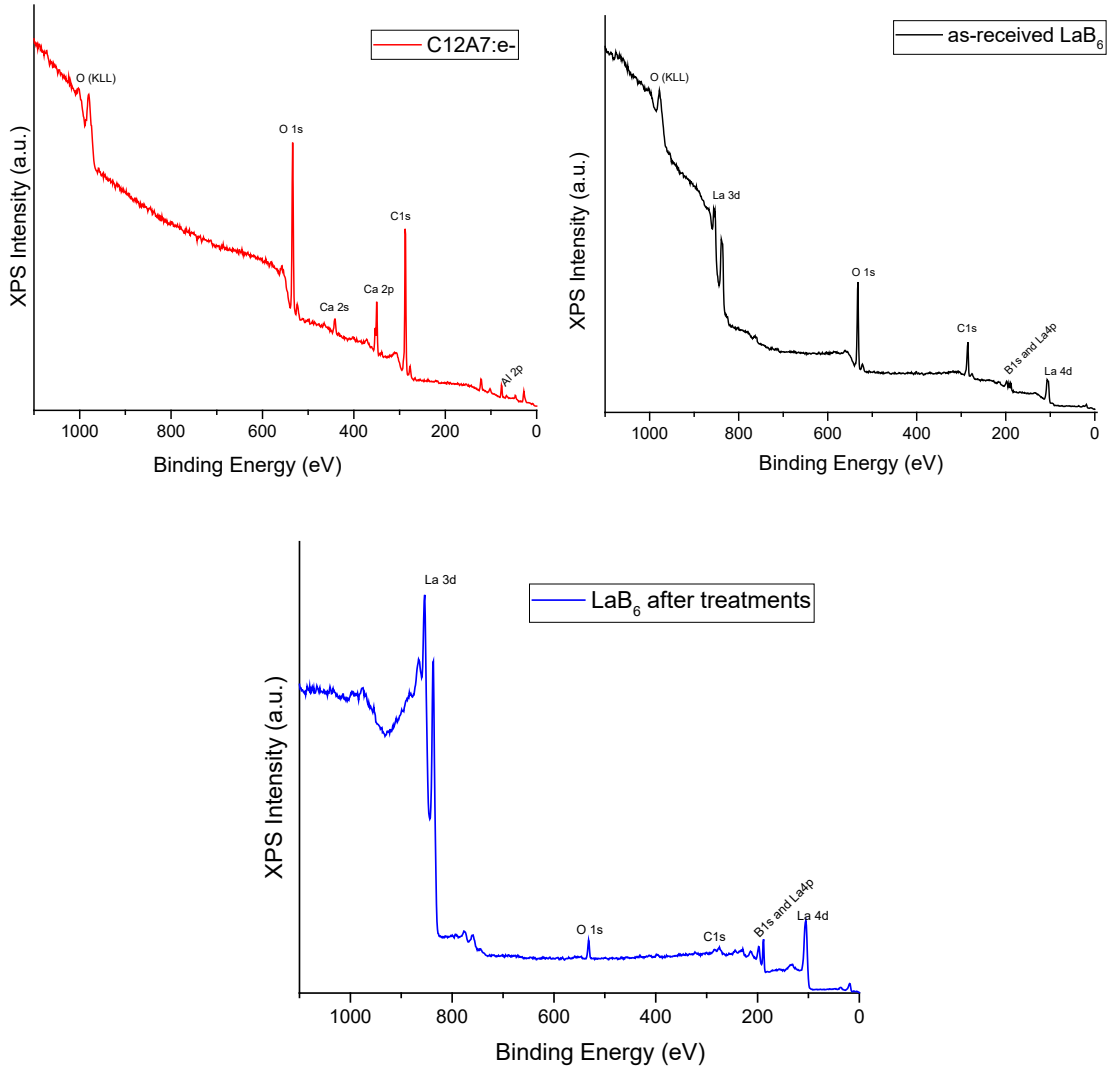

Fig. 12 Survey scan spectra of C12A7:e-, as received LaB_6 and LaB_6 after all treatments.

Table 3. Surface atomic ratios of all elements calculated from high-resolution XPS spectra.

Sample	C, %	O, %	B, %	La, %	Ca, %	Al, %
As received LaB6	40.1	41.3	12.0	6.6	-	-
LaB6 after all treatments*	5.1	10.2	63.1	21.6	-	-
C12A7:e-	58.8	30.4	0	0	4.7	6.1

*Ex-situ (chemical cleaning) and in situ (annealing overnight, Ar^+ sputtering, 3.5h).

High resolution XPS spectra were also obtained. Characteristic XPS spectra of the electride and LaB_6 are shown in Fig. 13. The surface of the non-treated samples is dominated by the C 1s and O 1s peaks (not shown) as is commonly the case for ex situ prepared samples. These species are probably induced from atmospheric contamination (i.e. adventitious carbon) and sample oxidation, prior to the XPS measurements, in the period that the samples were exposed in air. In the non-treated LaB_6 sample, the La 3d and B 1s signals (not shown) are characteristic for the LaB_6 phase. The shape of the La 3d peak, with the intense satellites at the high BE side, are typical for oxygen exposed La (lanthanum oxide). The position of the La 3d and B 1s peaks agree well with data for LaB_6 obtained in earlier reports [16]. In LaB_6 sample after treatments, the shape of the La 3d peak changes and is typical for a "clean" LaB_6 surface [17]. In the case of the electride, the Al 2p peak appears at 74 eV, which is characteristic of oxidized Al, and the Ca $2p_{3/2}$ peak at 347.1 eV.

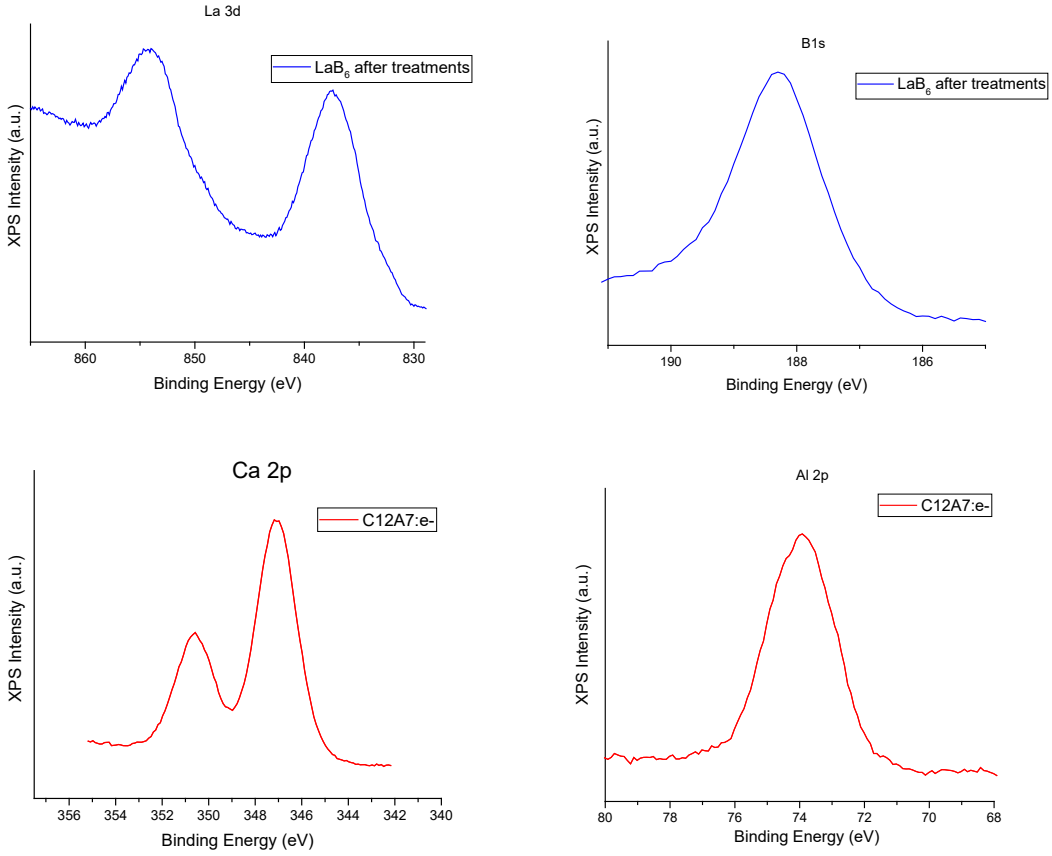

Fig. 13 Characteristic high resolution XPS spectra of C12A7:e- and LaB_6 samples.

C. Thermionic emission

In this section the raw data and the post-processed results of the thermionic emission setup are presented. Fig. 14 shows the raw data of (a) oxidised LaB_6 (LaB6-sample2) and (b) ATD's C12A7:e- (C12A7-sample2) at various sample temperatures. Note that C12A7:e- has the highest emitted current (leak current contribution not removed).

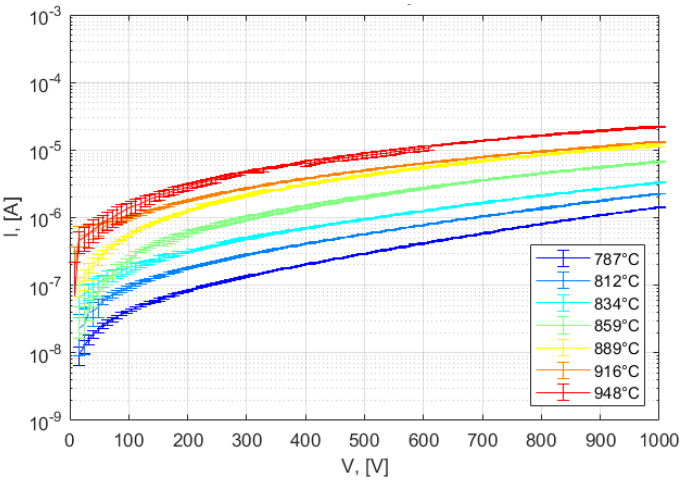

(a) LaB_6 (LaB6-sample2)

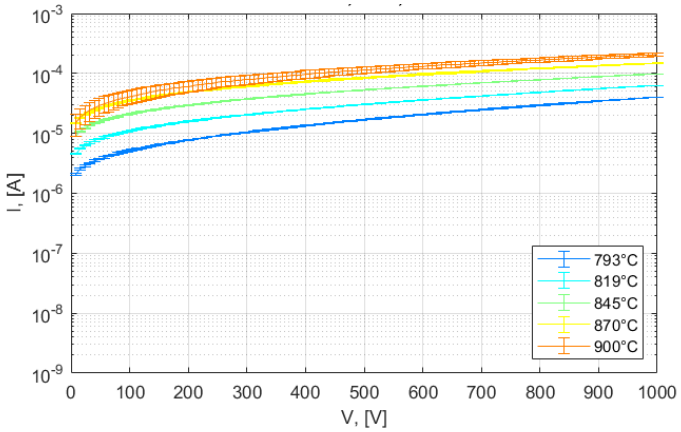

(b) C12A7:e- (C12A7-sample2)

Fig. 14 Raw I-V characteristics (leak current not subtracted) at various sample temperature.

The logarithm of the current as a function of the square root of the bias voltage is shown in Fig. 15. The linear fitting is performed using equation (5).

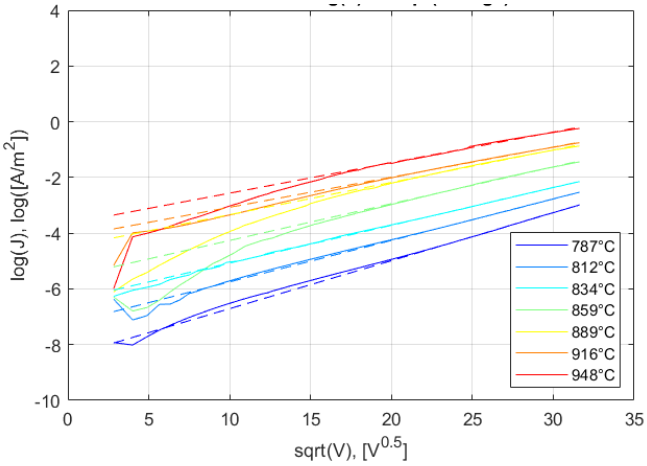

(a) LaB_6 (LaB6-sample2)

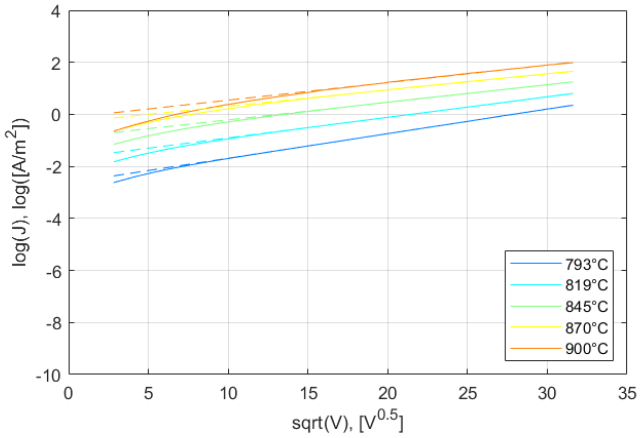

(a) C12A7:e- (C12A7-sample2)

Fig. 15 Fitting of the processed data as in equation (5) (leak current subtracted) .

The Richardson plots of the two samples are shown in Fig. 16. The dots represent the experimental data, the red line is the fitting curve with imposed $\beta = 0\ eV/K$, the blue line is the fitting curve where β is also fitting parameter together with ϕ_0.

A comparison of the Richardson plots of the two samples and that without sample – calculation made from the leak current – is shown in Fig. 17.

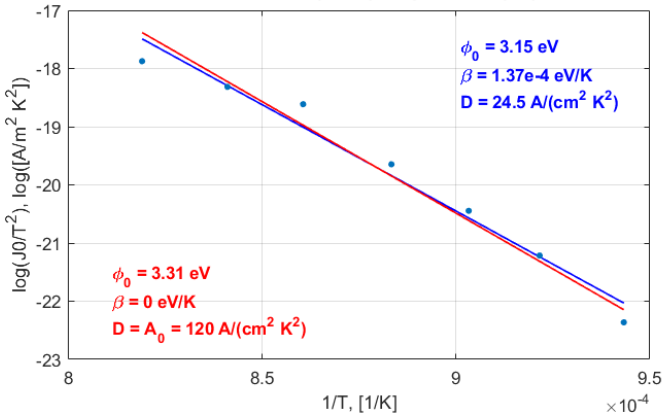

(a) LaB_6 (LaB6-sample2)

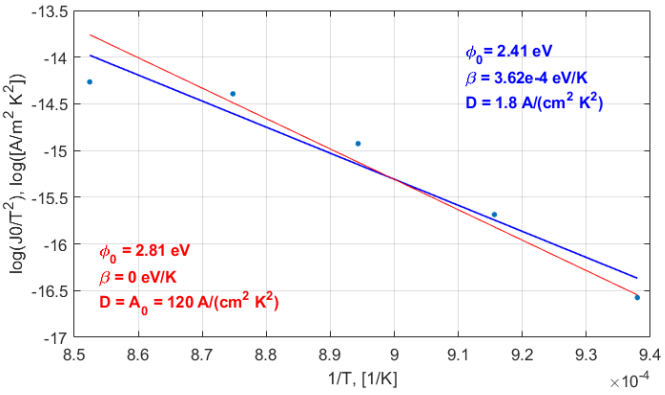

(a) C12A7:e- (C12A7-sample2)

Fig. 16 Richardson plots of the processed data, fitted according to equation (9) when $\boldsymbol{\beta = 0\ eV/K}$ (red line) and $\boldsymbol{\beta \neq 0\ eV/K}$ (blue line).

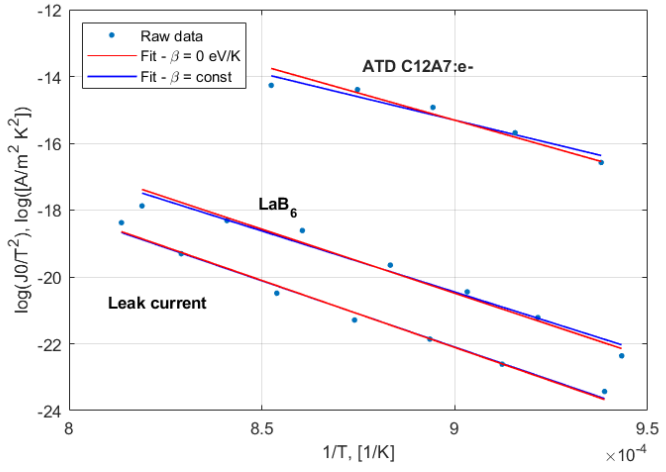

Fig. 17 Richardson plots of the two samples along with the leak current plot.

The work function and the Richardson coefficient of the tested samples, leak current and reference LaB_6 from literature [12] are listed in Table 4. The corresponding thermionic current density as a function of the temperature is shown from Fig. 18 to Fig. 20.

Table 4 Work function and Richardson coefficient of the tested samples, leak current and reference LaB_6 from literature.

	Reference equations: $\phi = \phi_0 + \beta T$ $D = A_0 \exp(-e\beta/k_B)$			
	Thermionic emission setup		UPS	Supplier's
Sample	Case $\beta = 0$ eV/K	Case $\beta \neq 0$ eV/K	Case $\beta = 0$ eV/K	-
LaB_6 Sample 1 and 2	Sample 2: $\phi = \phi_0 = 3.31$ eV (as received)	Sample 2: $\phi = 3.15 + 1.37 \cdot 10^{-4} T$ $D = 24.5$ A/(cm^{2}K^2) (as received)	Sample 1: $\phi = \phi_0 = 4.3$ eV (as received) $\phi = \phi_0 = 3.2$ eV (after 3.5h Ar^+ sputtering)	$\phi = \phi_0 < 4$ eV [18]
ATD, C12A7:e- Sample 1 and 2	Sample 1: $\phi = \phi_0 = 2.81$ eV	Sample 1: $\phi = 2.41 + 3.62 \cdot 10^{-4} T$ $D = 1.8$ A/(cm^{2}K^2)	Sample 2: $\phi = \phi_0 = 3.21$ eV	$\phi = \phi_0 = 2.4$ eV (theory)
LaB6 from [12]	-	$\phi = 2.66 + 1.23 \cdot 10^{-4} T$ $D = 29$ A/(cm^{2}K^2)	-	-
Leak current	$\phi = \phi_0 = 3.46$ eV	$\phi = 3.42 + 3.30 \cdot 10^{-5} T$ $D = 81.8$ A/(cm^{2}K^2)	-	-

The work function of the LaB_6 sample stated by the supplier is <4 eV. From UPS measurement, the "as received" sample's work function is about 4.3 eV, well above the value typically found in literature (2.66 eV [12]). XPS measurements have shown that the surface may be oxidised. After 3.5h of argon (Ar^+) sputtering, the surface's work function measured by UPS decreased to 3.2 eV. Thermionic emission measurements show a work function close to 3.31 eV (case $\beta = 0$ eV/K) and 3.25 eV ($\beta = 1.37 \cdot 10^{-4}$ eV/K, $D = 24.5$ A/(cm^{2}K^2)), without any surface treatment. See Fig. 18.

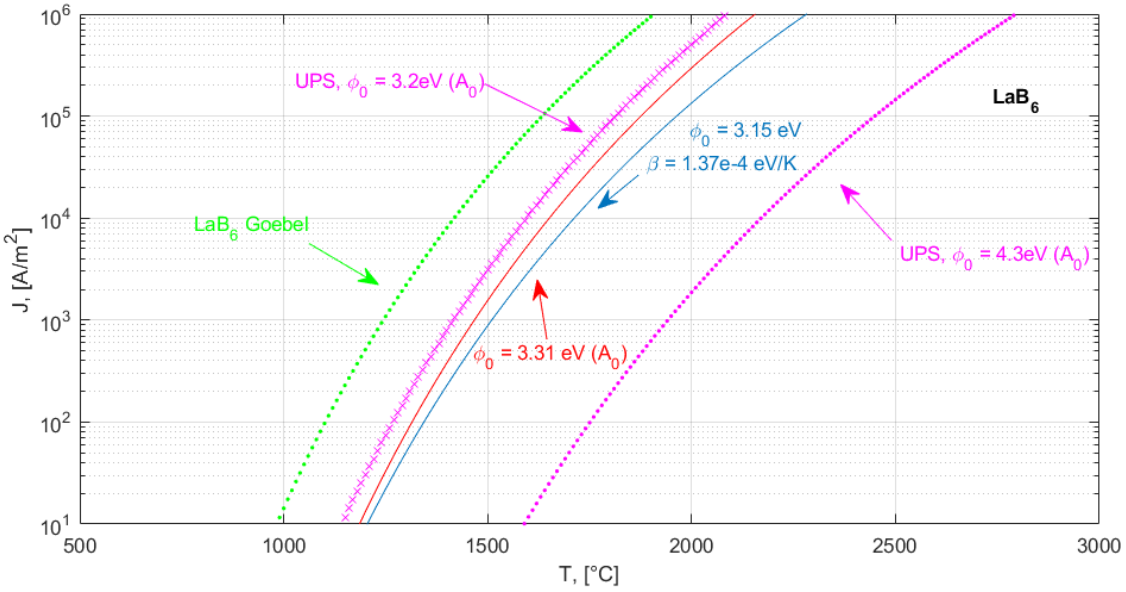

Fig. 18 Emission current density of LaB_6 according to thermionic emission (LaB6-sample2) and UPS (LaB6-sample1) measurements. As a reference, the emission curve of LaB_6 as in [12] **is showed in green (dotted line).**

The work function of the C12A7:e- as measured by UPS is about 3.21 eV, above the expected theoretical value of 2.4 eV. Thermionic emission measurements show a work function close to 2.81 eV (case $\beta = 0$ eV/K) and 2.41 eV ($\beta = 3.62 \cdot 10^{-4}$eV/K, $D = 1.8$ A/(cm^{2}K^2)). See Fig. 19.

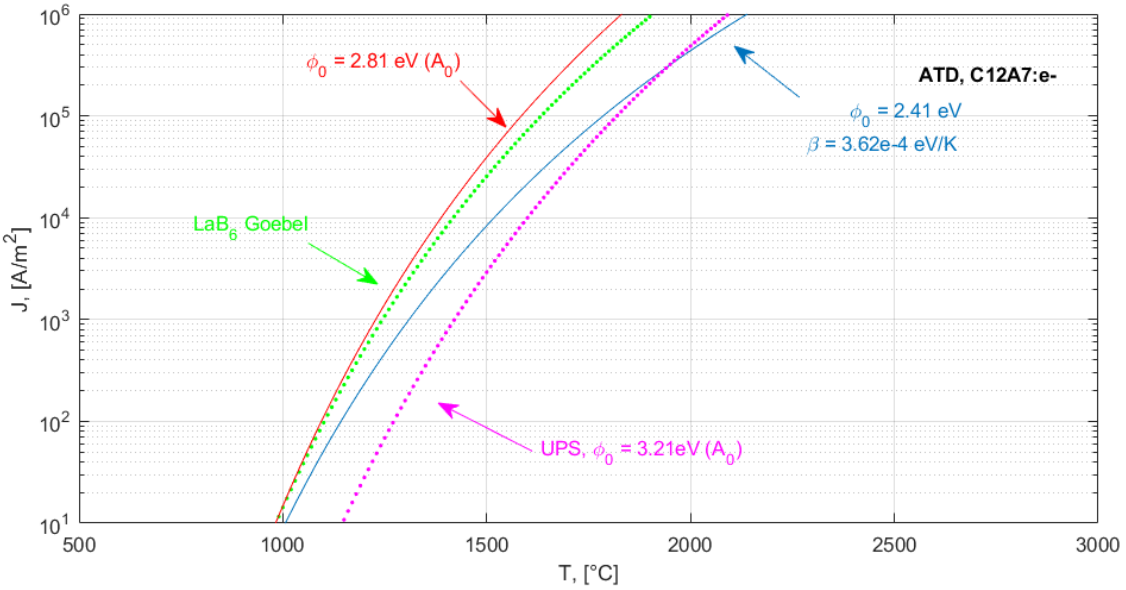

Fig. 19 Emission current density of the C12A7:e- according to thermionic emission (C12A7-sample2) and UPS (C12A7-sample1) measurements. As a reference, the emission curve of LaB6 as in [12] **is showed in green (dotted line).**

As a setup check, the intrinsic work function of the thermionic emission setup has been calculated (without sample). Thermionic emission measurements show a work function close to 3.46 eV (case $\beta = 0$ eV/K) and 3.42 eV

($\beta = 3.30 \cdot 10^{-5}$ eV/K, $D = 81.4$ A/(cm^{2}K^2)), see Fig. 20. This shows that the setup can influence the work function measurement if the leak current is not subtracted from the emission characteristics.

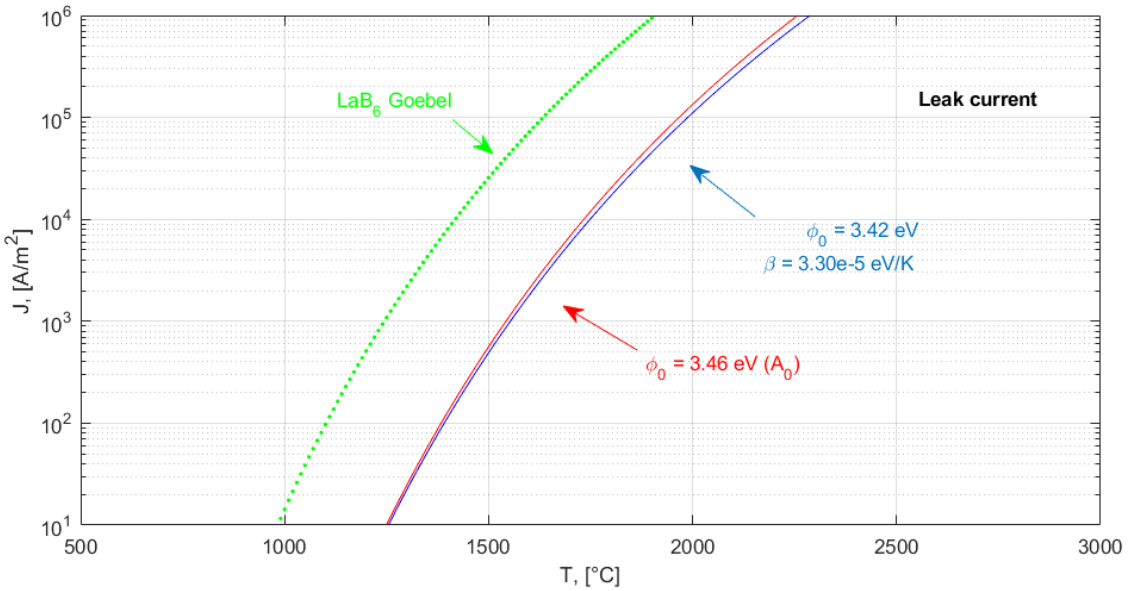

Fig. 20 Intrinsic emission current density of the thermionic emission setup. As a reference, the emission curve of LaB6 as in [12] **is showed in green (dotted line).**

VI. Conclusions

The work functions of LaB_6 and ATD's C12A7:e- have been estimated by thermionic emission measurements and compared with UPS data. Table 4 summarises the results. The estimation of the work function has been done using the Richardson-Dushman equation in the case where the work function is a function of ($\beta \neq 0$ eV/K) or independent from ($\beta = 0$ eV/K) the temperature.

For LaB_6, XPS tests have shown that the surface may be oxidised (work function of 4.3 eV). After 3.5h of argon (Ar+) sputtering, the surface work function measured by UPS decreased to 3.2 eV. Thermionic emission measurements show a work function close to 3.31 eV (case $\beta = 0$ eV/K) and 3.25 eV ($\beta = 1.37 \cdot 10^{-4}$ eV/K, $D = 24.5$ A/(cm^{2}K^2)), without any surface treatment. The sample (LaB6-sample2) darkened after thermionic emission tests. The sample (LaB6-sample1) that underwent UPS analysis and was subject to Ar+ sputtering has changed colour. This suggests the emerging of a non-stoichiometric boron-rich surface, above $LaB_{6.07}$ [19].

Regarding the C12A7:e- sample, the work function measured by UPS is about 3.21 eV, above the expected theoretical value of 2.4 eV. Thermionic emission measurements show a work function close to 2.81 eV (case $\beta = 0$ eV/K) and 2.41 eV ($\beta = 3.62 \cdot 10^{-4}$eV/K, $D = 1.8$ A/(cm^{2}K^2)). The emitting side did not change colour. However, the back of the sample, which is platinum coated, shows colour modification.

Acknowledgments

This project has received funding from the European Union's Horizon 2020 research and innovation program under grant agreement No 870506.

References

[1] D. R. Lev, I. G. Mikellides, D. Pedrini, D. M. Goebel, B. A. Jorns, and M. S. McDonald, "Recent progress in research and development of hollow cathodes for electric propulsion," *Rev. Mod. Plasma Phys.*, vol. 3, no. 6, 2019, doi: 10.1007/s41614-019-0026-0.

[2] S. Matsuishi *et al.*, "High-density electron anions in a nanoporous single crystal: [Ca24Al28O64]4+ (4e-)," *Science (80-.).*, vol. 301, no. 5633, pp. 626–629, 2003, doi: 10.1126/science.1083842.

[3] L. P. Rand and J. D. Williams, "A Calcium Aluminate Electride Hollow Cathode," *IEEE Trans. Plasma Sci.*, vol. 43, no. 1, pp. 190–194, 2015, doi: 10.1109/TPS.2014.2338737.
[4] Y. Toda *et al.*, "Field Emission of Electron Anions Clathrated in Subnanometer-Sized Cages in [Ca24Al28O64]4+(4e-)," *Adv. Mater.*, vol. 16, no. 8, pp. 685–689, 2004, doi: 10.1002/adma.200306484.
[5] Y. Toda *et al.*, "Intense thermal field electron emission from room-temperature stable electride," *Appl. Phys. Lett.*, vol. 87, no. 25, pp. 1–3, 2005, doi: 10.1063/1.2149989.
[6] Y. Toda *et al.*, "Work function of a room-temperature, stable electride [Ca24Al28O64]4+(e-) 4," *Adv. Mater.*, vol. 19, no. 21, pp. 3564–3569, 2007, doi: 10.1002/adma.200700663.
[7] M. Reitemeyer, D. Zschätzschy, K. Holste, L. Chen, and P. J. Klar, "Applicability of electride materials for hollow cathodes," in *36th International Electric Propulsion Conference*, 2019, no. 15-20 September, p. IEPC-2019-604.
[8] N. R. S. Caruso and M. S. McDonald, "Thermionic Emission Measurements of 12(CaO)-7(Al2O3) Electride in a Closed-Spaced Diode," in *35th International Electric Propulsion Conference*, 2017, no. 8-12 October, p. IEPC-2017-165.
[9] Y. Toda, Y. Kubota, M. Hirano, H. Hirayama, and H. Hosono, "Surface of room-temperature-stable electride [Ca24Al 28O64]4+(e-)4: Preparation and its characterization by atomic-resolution scanning tunneling microscopy," *ACS Nano*, vol. 5, no. 3, pp. 1907–1914, 2011, doi: 10.1021/nn102839k.
[10] T. Nagao, K. Kitamura, Y. Iizuka, and O. Chuhei, "Surface Science 290 (1993) 436-444.," *Surf. Sci. 290*, pp. 436–44, 1993.
[11] D. Briggs and M. P. Seah, "Briggs, D. and Seah, M.P. (1990) Practical Surface Analysis. Vol. 1," *Pract. Surf. Anal.*, vol. 1, 1990.
[12] D. M. Goebel and I. Katz, *Fundamentals of Electric Propulsion - Ion and Hall Thrusters*. Hoboken, New Jersey: John Wiley and Sons, 2008.
[13] W. Schottky, "Concerning the Discharge of Electrons from Hot Wires with Delayed Potential," *Ann. Phys.*, vol. 349, no. 15, pp. 1011–1032, 1914.
[14] J. A. Becker and W. H. Brattain, "The thermionic work function and the slope and intercept of Richardson plots," *Phys. Rev.*, vol. 45, no. 10, pp. 694–705, 1934, doi: 10.1103/PhysRev.45.694.
[15] M. Trenary, "Surface science studies of metal hexaborides," *Sci. Technol. Adv. Mater.*, no. 13, p. 023002, 2012.
[16] J. Xu *et al.*, "Fabrication of vertically aligned single-crystalline lanthanum hexaboride nanowire arrays and investigation of their field emission," *NPG Asia Mater.*, vol. 5, no. 7, pp. e53-9, 2013, doi: 10.1038/am.2013.25.
[17] C. L. Perkins, M. Trenary, T. Tanaka, and S. Otani, "X-ray photoelectron spectroscopy investigation of the initial oxygen adsorption sites on the LaB6(100) surface," *Surf. Sci.*, vol. 423, no. 1, pp. L222–L228, 1999, doi: 10.1016/S0039-6028(98)00936-4.
[18] Sindlhauser website, "https://www.sindlhauser.de/en/lab6-keramik-und-kathoden.html." .
[19] T. Lundstrom, "Structure, Defects and Properties of Some Refractory Borides.," *Pure Appl. Chem.*, vol. 57, no. 10, pp. 1383–1390, 1985, doi: 10.1351/pac198557101383.